

Calibration of IR Test Chambers with the Missile Defense Transfer Radiometer

Simon G. Kaplan, Solomon I. Woods
National Institute of Standards and Technology
Gaithersburg, MD 20899-8441

Adriaan C. Carter
Booz Allen Hamilton, Inc.
Rockville, MD 20852

Timothy M. Jung
Jung Research and Development Corp.
Washington, DC 20009

ABSTRACT

The Missile Defense Transfer Radiometer (MDXR) is designed to calibrate infrared collimated and flood sources over the fW/cm^2 to $\mu\text{W/cm}^2$ power range from $3\ \mu\text{m}$ to $28\ \mu\text{m}$ in wavelength. The MDXR operates in three different modes: as a filter radiometer, a Fourier-transform spectrometer (FTS)-based spectroradiometer, and as an absolute cryogenic radiometer (ACR). Since 2010, the MDXR has made measurements of the collimated infrared irradiance at the output port of seven different infrared test chambers at several facilities. We present a selection of results from these calibration efforts compared to signal predictions from the respective chamber models for the three different MDXR calibration modes. We also compare the results to previous measurements made of the same chambers with a legacy transfer radiometer, the NIST BXR. In general, the results are found to agree within their combined uncertainties, with the MDXR having 30 % lower uncertainty and greater spectral coverage.

Keywords: infrared, radiometry, calibration, cryogenics, transfer radiometer, Fourier-transform spectrometer

1. INTRODUCTION

The Low-Background Infrared (LBIR) facility at the National Institute of Standards and Technology (NIST) provides calibration of cryogenic blackbody sources used in infrared space simulation chambers [1, 2] as well as calibration of the irradiance output of these chambers through the use of portable transfer radiometers. The Ballistic Missile Defense Transfer Radiometer (BXR) has been in use since 2001, while the Missile Defense Transfer Radiometer (MDXR) has been used since 2010. The calibration and use of the BXR has been described previously [3, 4], along with the design [5] and preliminary calibration results [6] from the MDXR.

Both the BXR and MDXR include infrared filter-based radiometers covering the $3\ \mu\text{m}$ to $14\ \mu\text{m}$ spectral range. They are housed in vacuum cryogenic shells operating at a background temperature of 20 K and use Si:As blocked-impurity band (BIB) detectors operating at 10 K [7]. Their 7 cm diameter defining apertures are designed to sample the central portion of the collimated output beam from infrared test chambers, which can be as much as 50 cm in diameter. In addition to the filter-based radiometer, the MDXR has a cryogenic Fourier-transform spectrometer (CFTS) [8, 9] and an onboard absolute cryogenic radiometer (ACR) [2]. There is also a blackbody source that is used to provide a reference for the CFTS and a stability monitor for the filter radiometer and ACR. This gives the MDXR some capability for self-calibration in addition to continuous high-resolution spectral coverage out to $28\ \mu\text{m}$ wavelength. In this paper, we describe the calibration of the different operating modes of the MDXR and illustrate its use in transferring the LBIR irradiance scale to users' infrared test chambers.

2. MDXR OPTICAL DESIGN

Figure 1 below shows the entrance beam optical layout of the MDXR when viewing (a) its own internal blackbody source or (b) an external source. The blue arrows indicate the incident beam directions.

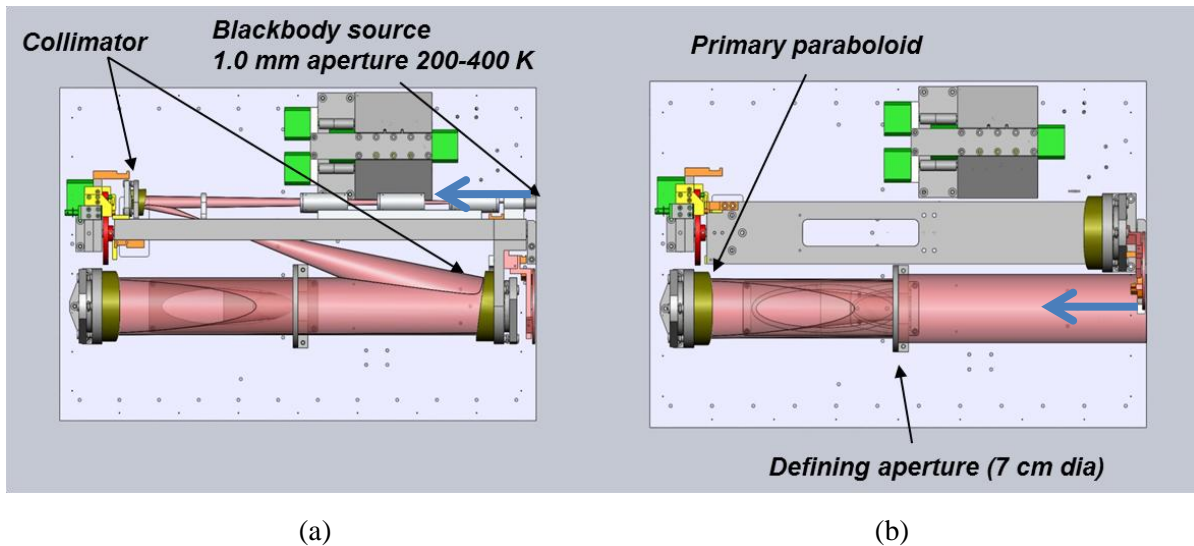


Figure 1. Schematic layout of input optics and defining aperture of the MDXR on one side of the vertically oriented cryogenic optics plate. The radiometer views either (a) the internal blackbody through a two-mirror collimator that produces a 7 cm diameter beam incident on the defining aperture, or (b) the external collimated source under test.

When viewing an external source, the input beam passes (from right to left in Figure 1(b)) through the 7 cm diameter defining aperture and then strikes the primary paraboloidal mirror, which directs the beam to the other side of the vertically-oriented optics plate where it passes through a variable field stop wheel. In order to view the internal blackbody source, a two-mirror collimator is rotated into place and a blank plate is used to cover the entrance port of the radiometer. The primary focus of the collimator is at the 1 mm diameter defining aperture of the blackbody source, and a series of baffles limits the collimator view of any flux not coming directly from the blackbody aperture. A top view of the beam path coming from an external source is shown below in Figure 2.

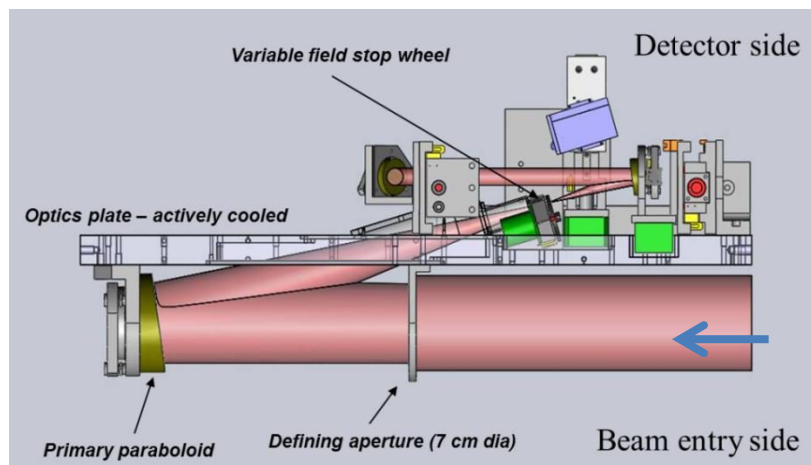


Figure 2. Top view of input beam path through the MDXR, with blue arrow indicating incident beam direction.

After passing through the variable field stop wheel, the beam is recollimated and directed toward a translating periscope assembly, then through a set of 4 filter wheels, after which the beam is brought to a focus in the region of a 3.2 mm square BIB detector as shown in Figure 3. The BIB detector is mounted on a three-axis translation stage and is typically positioned such that the entrance pupil of the instrument is imaged on the detector. This produces a beam spot approximately 2 mm in diameter which reduces the irradiance incident on the detector, improving signal response linearity and allowing the MDXR to receive 5 to 10 times more infrared flux than the BXR, which only images at infinity. The filter wheels contain short and long pass filters covering the 3 μm to 13 μm spectral region, and can be combined to produce band widths from 0.3 μm to as much as 6 μm [5]. There are also fixed vertical and horizontal linear polarizers as well as a rotatable polarizer that can be used to analyze the polarization content of the input beam.

The periscope is moved vertically to allow the recollimated input beam to pass into the CFTS. The CFTS has a KBr beamsplitter and porch swing moving mirror design [8] that provides spectral coverage from 3 μm to 28 μm wavelength with a highest spectral resolution of 0.85 cm^{-1} . After passing through the CFTS, the beam passes through the filter wheel assembly, allowing polarization analysis of the signal as well as the use of neutral density filters to limit the flux reaching the detector. In addition, the CFTS is used to make in-situ measurements of the filter band transmittances. Finally, the ACR can be moved to intercept the input beam just after the field stop, thus allowing absolute spectrally integrated flux measurements of the external source after only a single reflection from the primary mirror.

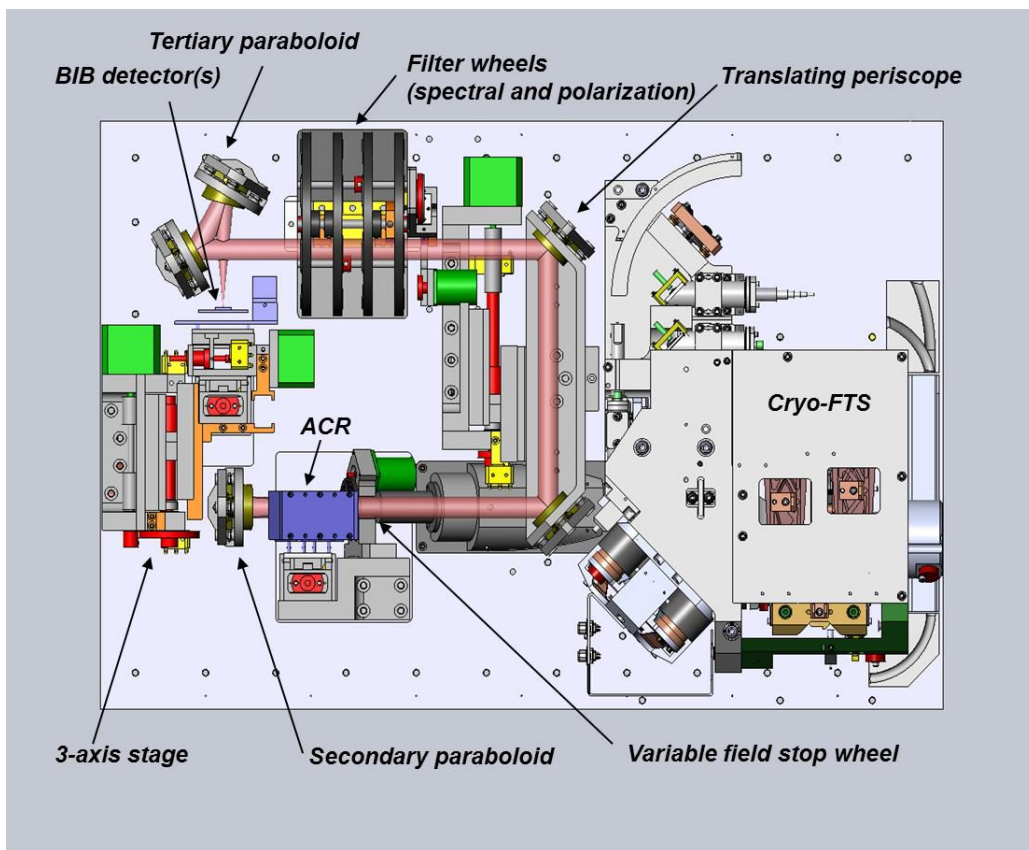


Figure 3. Detector side view of MDXR optical layout, showing the ACR, CFTS, filter wheel assembly, and detector with focusing mirror.

3. CALIBRATION OF THE MDXR

3.1 Filter radiometer calibration

The Ten Centimeter Collimator (10CC) chamber at NIST was used as the calibration source for the MDXR filter radiometer. Figure 4 shows the MDXR attached to the 10CC, viewing the output collimated beam which originates from the 10CC blackbody source and passes through a filter set that is nominally identical to that contained in the MDXR. A very similar approach was used for the calibration of the MDXR filter radiometer, to what was done for the BXR [4]. The biggest difference is the use of the ACR inside the MDXR, instead of the ACR located in the LBIR broadband chamber that was used for the BXR calibration. This resulted in a reduction in the type-B uncertainty components related to the radiometric defining aperture geometry, because now the same defining aperture is used for both the ACR and filter/BIB detector measurements. In addition, the ACR data acquired with the MDXR were used to improve the spectral throughput and blackbody calibration models of the 10CC through an iterative process. Lower calibration uncertainties were achieved for the MDXR than had previously been achieved for the BXR.

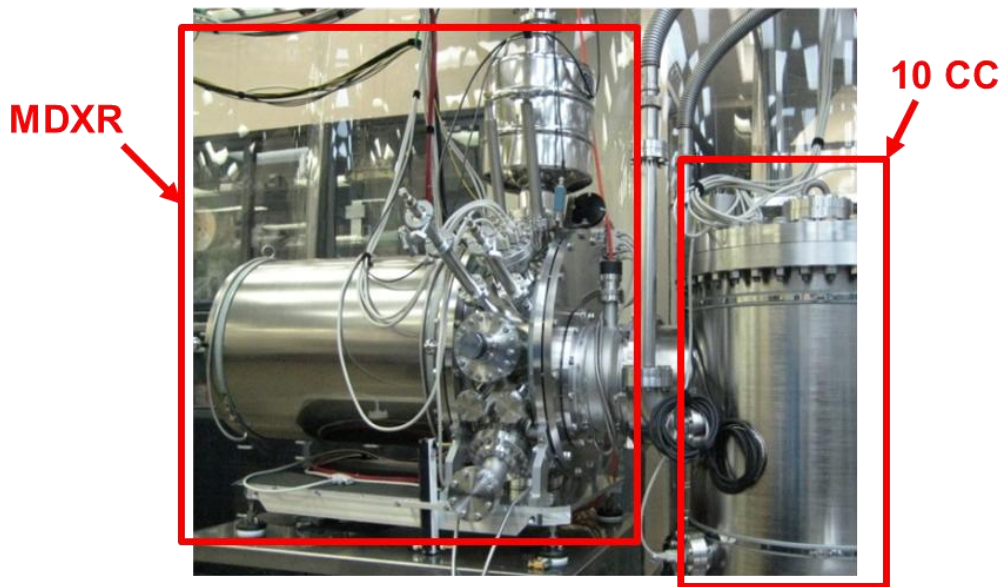


Figure 4. MDXR viewing the collimated output beam from the NIST 10CC chamber in order to calibrate the filter radiometer.

Data were collected using the ACR inside the MDXR at several temperature settings of the 10CC blackbody from 180 K to 600 K. The filter bandpasses on the 10CC were configured to the same set of bands that are used in the filter radiometer when calibrating a user chamber. Measurements of beam power sampled by the MDXR 7 cm diameter aperture made with the ACR only include uncertainties from the ACR (< 0.1 % combined power measurement uncertainty), a single mirror reflection from the high reflectance Au primary mirror (≈ 0.4 % reflectance uncertainty), and diffraction (≈ 0.5 % uncertainty). Calibration coefficients C for the 10CC model are calculated as

$$1 \approx C(10CC)_i = \frac{(ACR_Signal)_i}{G_{ACR}^{10CC} \int_0^{\infty} P_{10CC}(T, \lambda) \gamma_{10CC}(\lambda) \tau_i(\lambda) R_{PRI}(\lambda) D_{ACR}^{10CC}(\lambda) d\lambda} \quad (1)$$

The denominator in Eq. 1 is the signal predicted by the model of the 10CC and ACR functioning together. The term G is the geometric optical configuration factor between the 10CC and the ACR. P is the 10CC blackbody source model irradiance equation, γ is the spectral throughput of the 10CC including all the optical components from the blackbody cavity to the final pointing mirror, τ_i is the transmission through 10CC spectral filter i , $R_{PRI}(\lambda)$ represents the single MDXR mirror reflection between the 10CC output port and the ACR, and D is the diffraction correction for the 10CC and MDXR optical systems operating together. Since the signal measured by the ACR extends to very long wavelength ($\approx 600 \mu\text{m}$), the 10CC model must be extrapolated to long wavelength to compare with the data.

Once these calibration coefficients are applied to the 10CC model, its output power can be used to calibrate the filter radiometer. This comparison is made in the form of a similar calibration equation

$$1 \approx C(\text{MDXR})_i = \frac{(\text{MDXR_Signal})_i}{C(\text{10CC})_i G_{\text{MDXR}}^{10\text{CC}} \int_0^{\infty} P_{10\text{CC}}(T, \lambda) \gamma_{10\text{CC}}(\lambda) \tau_i(\lambda) R_{\text{MDXR}}(\lambda) D_{\text{MDXR}}^{10\text{CC}}(\lambda) d\lambda} \quad (2)$$

The term $C(\text{10CC})_i$ is the 10CC calibration factor when spectral filter i is placed in the optical path. R_{MDXR} is the MDXR spectral response model with no filter in the beam path, which includes both the mirror transmission and BIB detector responsivity in A/W. The resulting MDXR calibration coefficients and associated uncertainties are shown below in Figure 5.

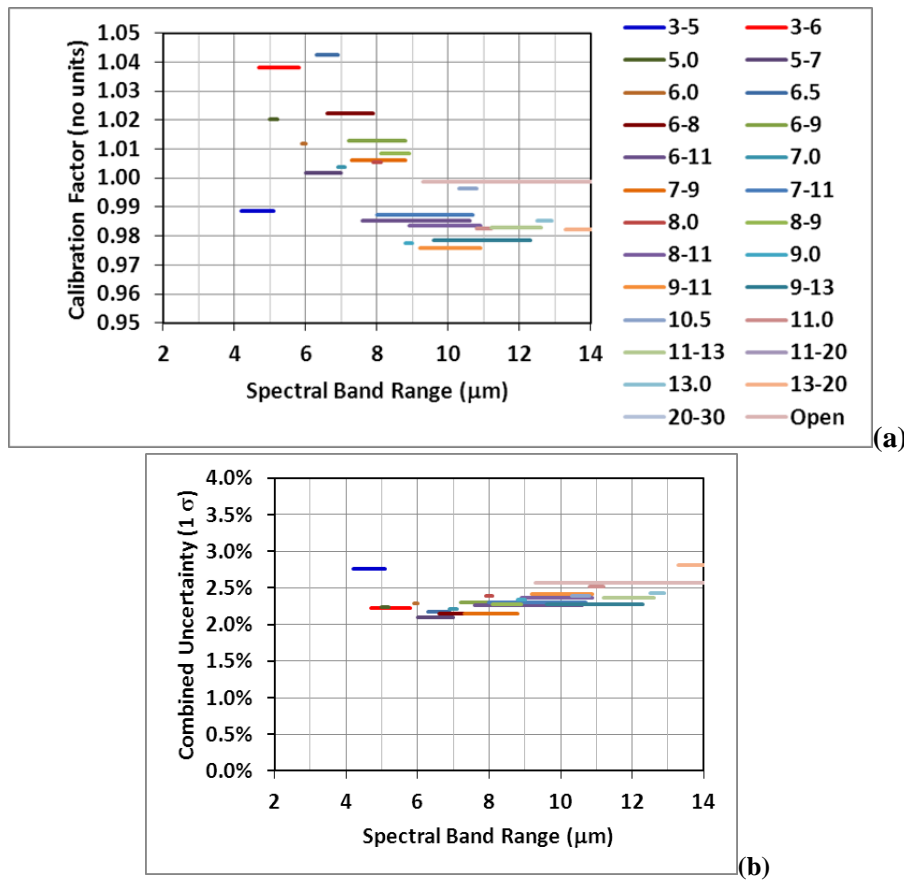


Figure 5. (a) Radiometric calibration coefficients and (b) associated uncertainties ($k=1$) for the MDXR response model derived from measurements of the 10CC source as discussed in the text. The horizontal extent of the lines represents the approximate width of each of the MDXR filter bands (in μm).

The radiometric uncertainty (k=1) in the MDXR filter radiometer is thus between 2 % and 2.5 % over most of its spectral bands, compared to the approximately 3.5 % that was achieved over a similar wavelength range with the BXR. When the MDXR makes measurements of a user infrared chamber output, calibration coefficients for the infrared test chamber $C(ITC)_i$ are derived in a similar manner to Eq. 2, with the 10CC terms replaced by terms appropriate to the user chamber and $C(10CC)_i$ replaced with $C(MDXR)_i$. The final calibration uncertainties for the user chamber depend upon the repeatability of the measurements as well as a calibration transfer uncertainty term that accounts for the band integrated difference in the MDXR responsivity between the user chamber and 10CC output models.

3.2 CFTS calibration

Measurements of the user chamber spectral power collected by the MDXR 7 cm diameter defining aperture, $I_{ITC}(\lambda)$, are performed with the CFTS by ratioing on a wavelength by wavelength basis the spectra obtained from the user chamber source to those obtained from the internal reference blackbody contained in the MDXR (typically set to a temperature of 400 K):

$$I_{ITC}(\lambda) = \left(\frac{CFTS_Signal_ITC(\lambda)}{CFTS_Signal_BB(\lambda)} \right) G_{MDXR}^{BB} P_{BB}(T, \lambda) \gamma_{COLL}(\lambda) D_{MDXR}^{BB}(\lambda) \quad (3)$$

where G is the optical configuration factor between the MDXR blackbody source and the defining 7 cm entrance aperture of the MDXR, P is the Planck radiance, γ is the spectral throughput of the blackbody and two-mirror internal MDXR collimator, and D is the diffraction correction factor for the CFTS viewing the blackbody source. Background spectra with the MDXR shutter closed generally show signals below the noise floor out to beyond 13 μm wavelength. The background-corrected spectra are then compared with the user chamber model as in Eq. 2 to obtain spectral calibration factors

$$1 \approx C_{ITC}(\lambda) = \frac{I_{ITC}(\lambda)}{G_{MDXR}^{ITC} P_{ITC}(T, \lambda) \gamma_{ITC}(\lambda) D_{MDXR}^{ITC}(\lambda)} \quad (4)$$

Because both the user chamber irradiance and the responsivity of the MDXR are potentially polarization dependent, a subset of radiometric measurements are typically taken with horizontal or vertical polarizers in the beam path for both the internal blackbody and external (user chamber) source measurements. The γ_{COLL} term in in Eq. (3) is modified to take into account the slight (0.03 %) polarization induced by the two reflections in the internal MDXR collimator. These polarized measurements are summed and compared with the unpolarized measurements taken for the same user chamber conditions.

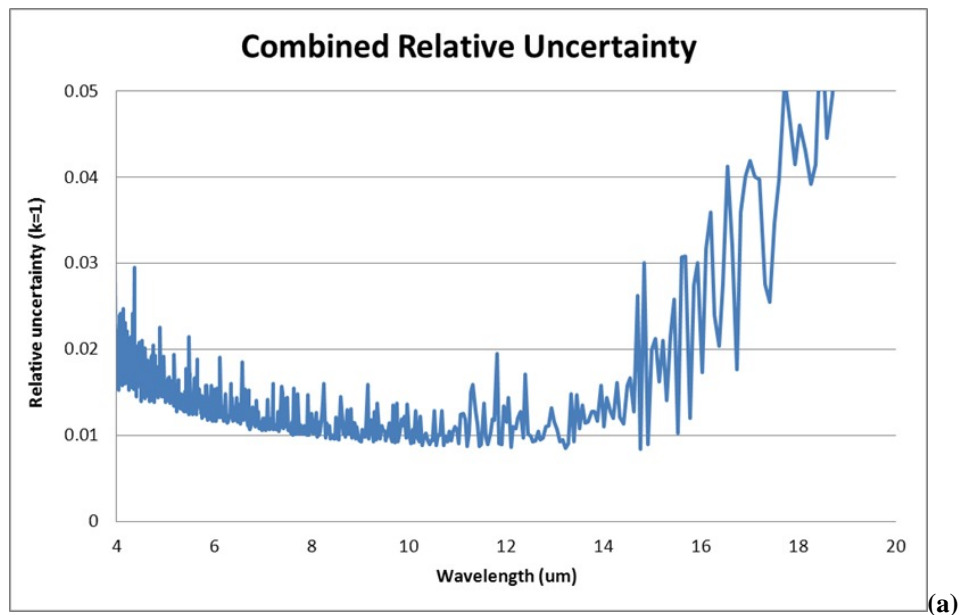
The uncertainties in the CFTS spectral irradiance measurements are evaluated by considering the repeatability of spectra acquired for both the internal blackbody source and the user source under test, where multiple test data are available, as well as the properties of the internal blackbody source and systematic sources of error in the CFTS. The internal blackbody source in the MDXR was observed with the ACR to determine its radiometric temperature at different temperature set points. At 400 K, the radiometric temperature was found to agree within 0.6 K uncertainty with the set point temperature.

We have estimated the relative uncertainty components for each of the Type-A (random, statistical) or Type-B (all other) sources, which are listed in Table 1 below at a wavelength of 10 μm . An example of the spectral dependence of the combined relative uncertainty is displayed in Figure 6(a). This uncertainty is multiplied by the observed user spectrum and then added in quadrature to the absolute uncertainty component due to noise in the detector/amplifier, which is shown in Figure 6(b) as apparent power received at the defining aperture of the MDXR (area = 38.5 cm^2). This produces a final expanded uncertainty (k=1) in the observed spectral power. In comparing to the model for a given source, we combine this uncertainty with the model uncertainty. For the case of the CFTS measurements of user chamber sources, the model uncertainty only

includes the uncertainty in received spectral power due to diffraction effects in the MDXR. The wavelength uncertainty of the CFTS is 0.05 %.

Relative uncertainty source	Value at 10 μm
Internal BB stability (type A)	0.0035
User source stability (type A)	0.002
Detector nonlinearity (type B)	0.0025
Alignment internal/external (type B)	0.001
Polarization correction (type B)	0.003
Defining aperture area (type B)	0.00007
Internal collimator geometry (type B)	0.001
Internal collimator diffraction correction (type B)	0.0018
Internal collimator mirror reflectance (type B)	0.007
Internal BB temperature (type B)	0.0046
Internal BB emissivity (type B)	0.001
Quadrature sum	0.010

Table 1. Estimated uncertainties in CFTS measurement of a user source referenced to the MDXR internal blackbody source.



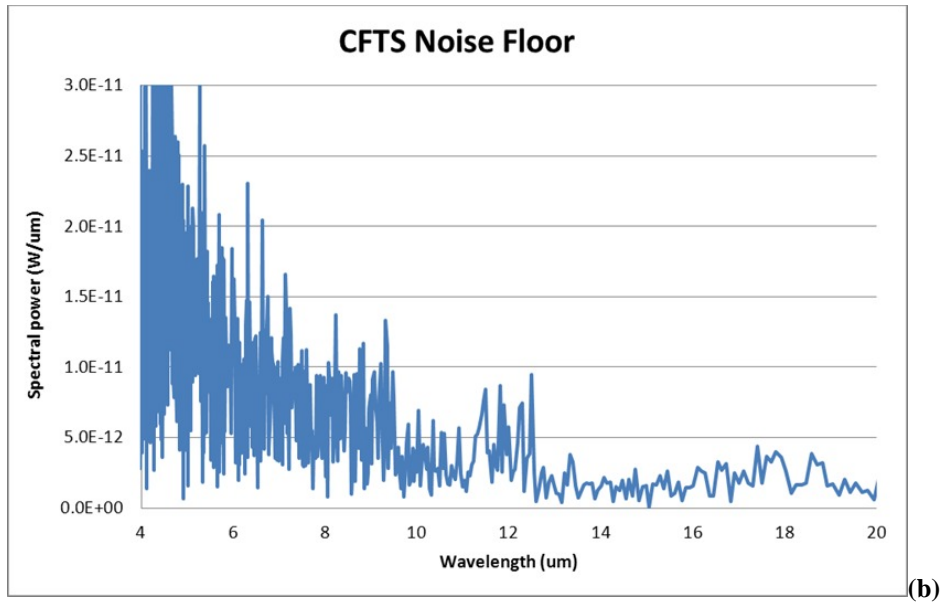
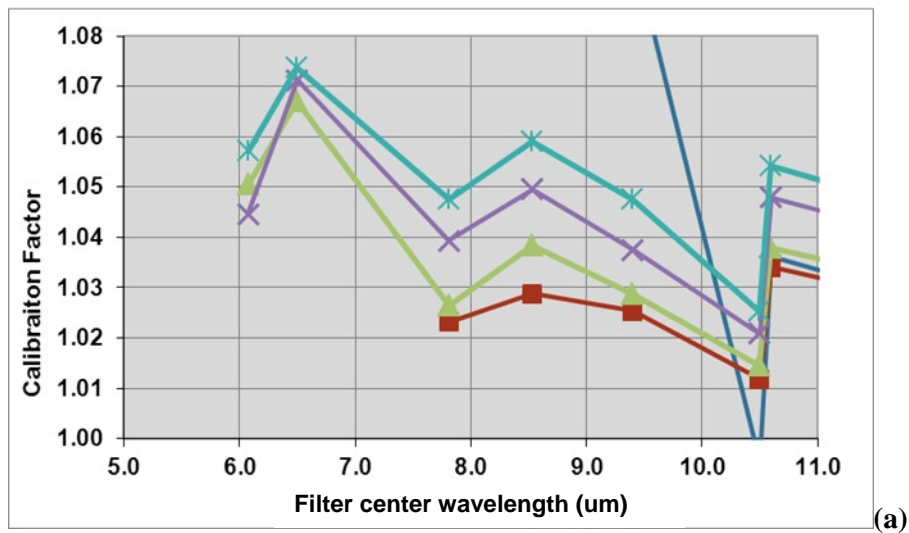


Figure 6. Spectral dependence of (a) the relative radiometric uncertainty and (b) the MDXR noise floor of a user source measured with the CFTS.

4. EXAMPLES OF USER TEST CHAMBER CALIBRATION RESULTS

The MDXR has been used to measure the output irradiance from several infrared test chambers at user sites which have previously been measured using the BXR. The data in this section are presented as the ratio of the measured signals from the MDXR to those predicted by a model similar to Eq. (2) or (4) for each chamber. The source geometry, source radiance temperature calibration, chamber optical throughput, effective focal length, and diffraction correction for the MDXR viewing geometry are combined with the calibrated MDXR responsivity model to calculate the expected signal for different wavelength bands. In Figure 7 below, we show the results for one particular chamber, denoted by Chamber X. This chamber was visited by the BXR and then by the MDXR shortly thereafter.



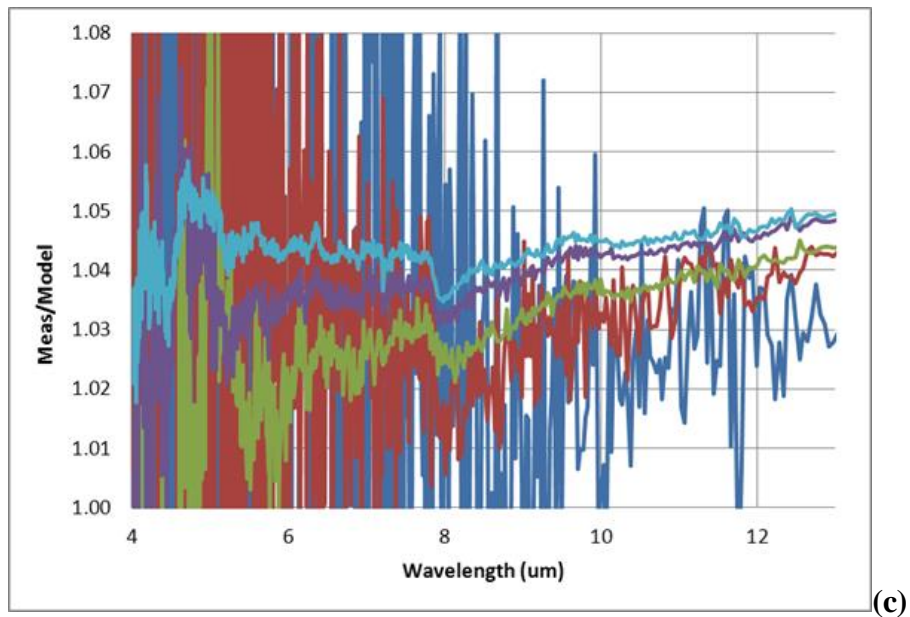
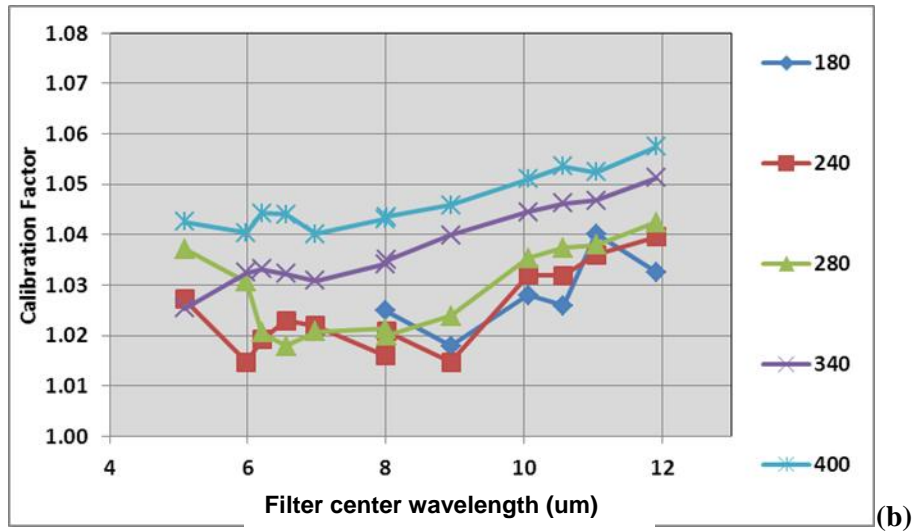


Figure 7. Ratio of measured to modeled signals for infrared test Chamber X as viewed by (a) the BXR, (b) the MDXR filter radiometer, and (c) the MDXR CFTS. Each curve corresponds to the blackbody source set point temperature in the legend of frame (b).

Each curve in this figure corresponds to calibration factor results for the blackbody source set point temperature shown in the legend, between 180 K and 400 K. The measurement uncertainties ($k=1$) in the BXR calibration factor data in Figure 7(a) range from 0.035 to 0.045, while the MDXR uncertainties for the data in (b) are in the range 0.025 to 0.030. It can thus be seen that the BXR and MDXR filter radiometer data on this user chamber agree with each other to within their combined uncertainties. The largest difference, of approximately 0.04, occurs near 6.5 μm wavelength. The overall trend versus temperature is similar in frames (a) and (b), while the trend versus wavelength is smoother in the MDXR results of frame (b). Figure 7(c) shows the results for this chamber using the CFTS in the MDXR. Here we see better agreement with the filter radiometer results from frame (b), with the differences being mostly about 0.01. The wavelength trends in (b) and (c) are similar, and likely more reliable than the BXR results for this chamber. The lower signal-to-

noise ratio of the CFTS at 8 cm^{-1} resolution compared to the filter radiometer is apparent in these data; however its increased resolution is able to discern a spectral dip near $8 \mu\text{m}$ probably related to the chamber mirror reflectance.

A comparison of the measurement uncertainties versus wavelength for the Chamber X data from Figure 7 is shown below in Figure 8. It can be seen that the CFTS can achieve somewhat lower uncertainty than the filter radiometer for the highest signal levels, but for lower temperature (or smaller source aperture) the noise in the CFTS dominates its measurement uncertainty. The filter radiometer has a noise floor which is approximately 2 orders of magnitude lower than the CFTS.

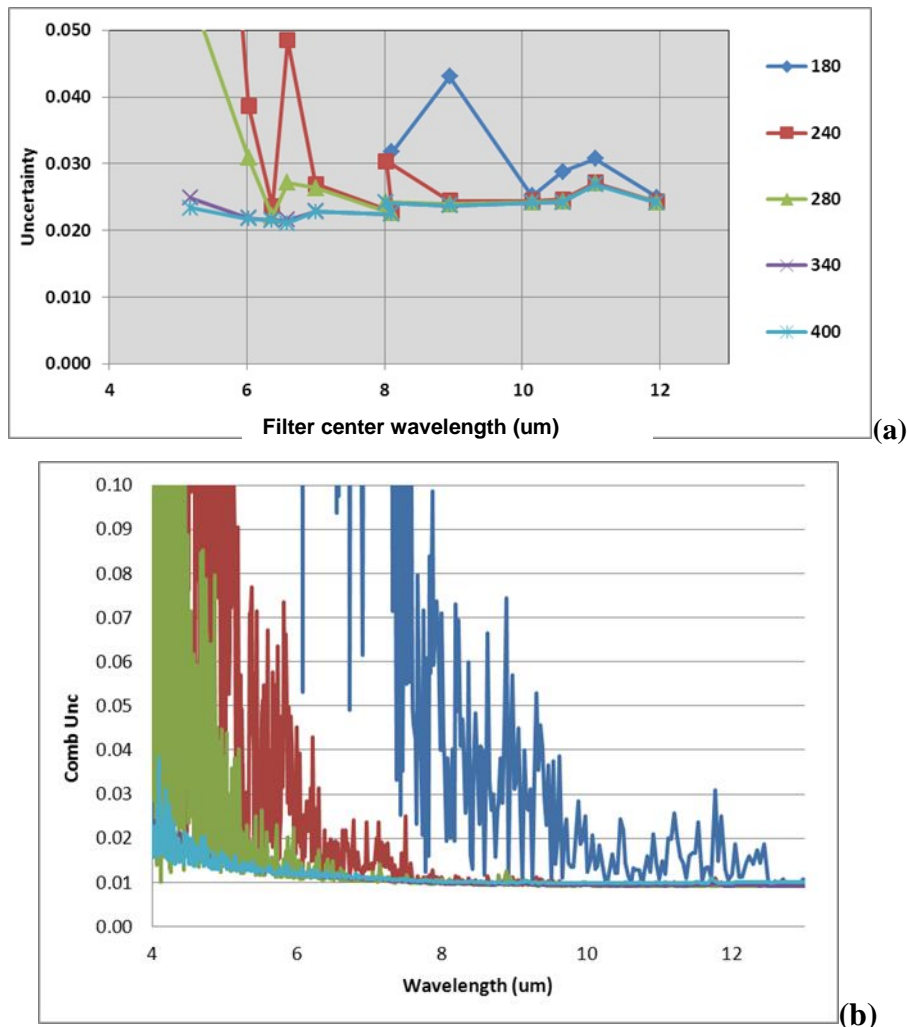


Figure 8. Measurement uncertainties in the (a) filter radiometer and (b) CFTS data from the MDXR measurements of Chamber X shown in Figure 7.

In Figure 9 below, we show the calibration factors measured for another chamber (called Chamber Y) with the MDXR filter radiometer and CFTS. This example shows less variation from the model as a function of blackbody set point temperature, but somewhat more variation as a function of wavelength. The added complexity of Chamber Y compared to Chamber X is a coated dielectric beam combiner optic, whose spectral properties may vary somewhat from the assumed model inputs. The periodic $\approx 1 \%$ spectral structure seen in the CFTS curves may result from frozen adsorbed gases on the MDXR optics, a result that has not been seen in data from other chambers. Overall there is again excellent agreement between the filter radiometer and

CFTS data. This agreement helps to validate the ACR-based scale of the filter radiometer versus the blackbody source-based scale of the CFTS.

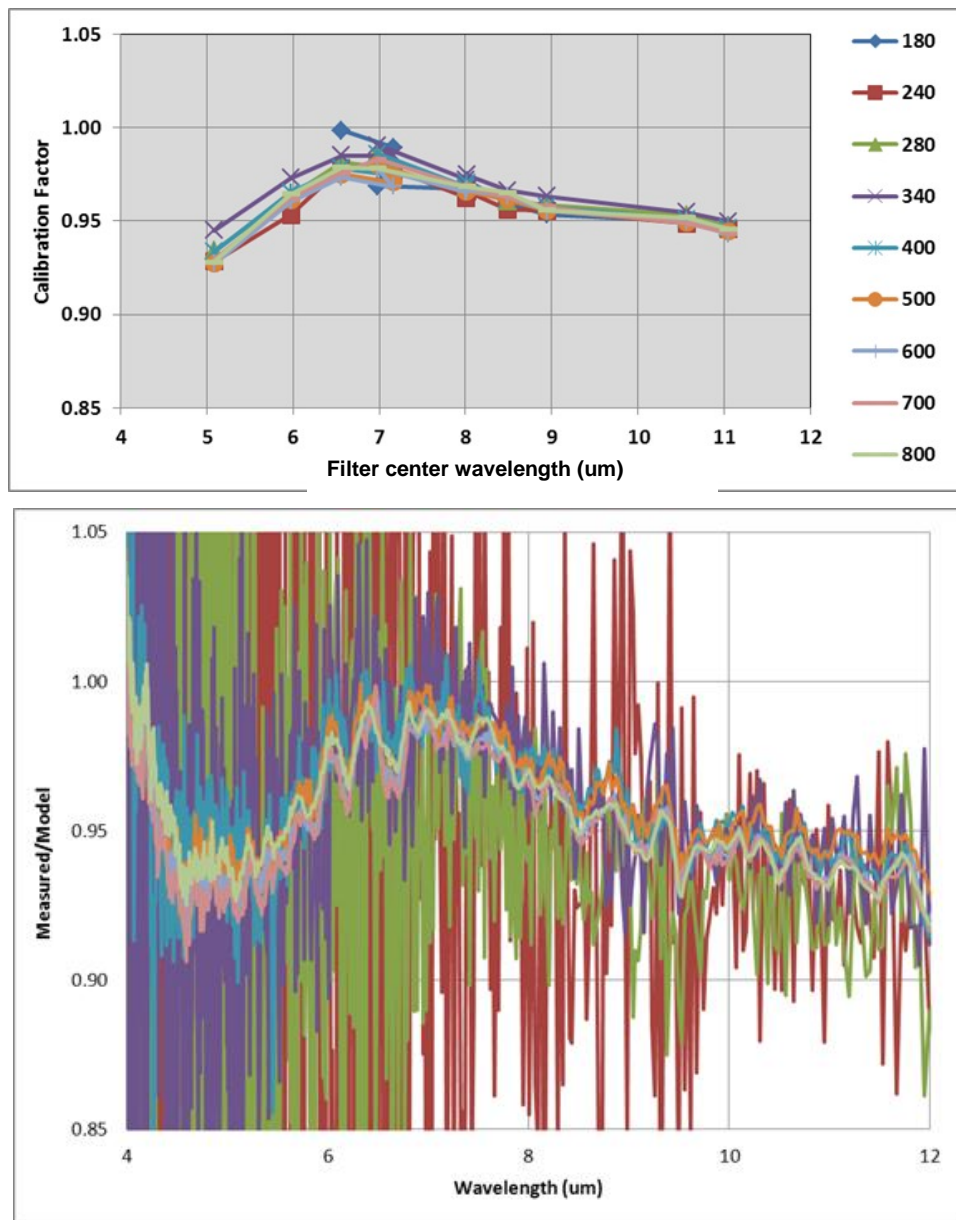


Figure 9. Ratio of measured to modeled signal for output of Chamber Y measured by the (a) MDXR filter radiometer and (b) CFTS for one source aperture setting and the series of blackbody set point temperatures shown in the legend.

5. CONCLUSIONS

The NIST low-background infrared irradiance scale, realized using an ACR to view a filtered blackbody source through a vacuum cryogenic collimator, has been successfully transferred to users' infrared test chambers using both the BXR and MDXR transfer radiometers. The MDXR has achieved approximately 30 % lower uncertainties than the BXR over the 3 μm to 13 μm wavelength range. Using the onboard CFTS, the MDXR can also provide calibrations with continuous spectral coverage out to 28 μm wavelength.

6. REFERENCES

1. R.U. Datla, K. Stock, A.C. Parr, C.C. Hoyt, P.J. Miller and P.V. Foukal, "Characterization of an absolute cryogenic radiometer as a standard detector for radiant-power measurements," *Appl. Opt.* **31**(34), 7219-7225 (1992).
2. Adriaan C. Carter, Steven R. Lorentz, Timothy M. Jung and Raju U. Datla, "ACR11: Improved absolute cryogenic radiometer for low background infrared calibrations," *Appl. Opt.* **44**(6), 871-875 (2005).
3. Timothy M. Jung, Adriaan C. Carter, Steven R. Lorentz, and Raju U. Datla, "NIST-BMDO Transfer Radiometer (BXR)," *Proc. of SPIE* **4028**, 404-410 (2000).
4. Adriaan C. Carter, Raju U. Datla and Timothy M. Jung, "Calibration of low-temperature IR test chambers used to calibrate space sensors," *Metrologia* **46**, S213-218 (2009).
5. Timothy M. Jung, Adriaan C. Carter, Solomon I. Woods, Simon G. Kaplan, and Raju U. Datla, "Infrared transfer radiometer for broadband and spectral calibration of space chambers," *Proc. of SPIE* **7663**, 76630J-1 to 76630J-9 (2010).
6. Timothy M. Jung, Adriaan C. Carter, Solomon I. Woods, and Simon G. Kaplan, "Calibration and Deployment of a New NIST Transfer Radiometer for Broadband and Spectral Calibration of Space Chambers (MDXR)," *Proc. of SPIE* **8015**, 80150C-1 to 80150C-10 (2011).
7. Adriaan C. Carter, Steven R. Lorentz, Timothy M. Jung, Beverly J. Klemme and Raju U. Datla, "NIST Facility for spectral calibration of detectors: calibration of arsenic doped silicon blocked impurity band detectors," *Proc. of SPIE* **4028**, 420-425 (2000).
8. Philippe Lagueux, Martin Chamberland, Frédérick Marcotte, André Villemaire, Marc Duval, Jérôme Genest, and Adriaan Carter, "Performance of a cryogenic Michelson interferometer," *Proc. of SPIE* **6692**, 669209-1 to 669209-11 (2007).
9. Simon G. Kaplan, Solomon I. Woods, Timothy M. Jung and Adriaan C. Carter, "Cryogenic Fourier Transform Infrared Spectrometer from 4 to 20 Micrometers," *Proc. of SPIE* **7739**, 77394D-1 to 77394D-8 (2010).